

Ultrafast optical bleaching of intersubband cavity polaritons

Simone Zanotto,* Riccardo Degl'Innocenti, Ji-Hua Xu, Lucia Sorba, and Alessandro Tredicucci
NEST, Istituto Nanoscienze–CNR and Scuola Normale Superiore, Piazza S. Silvestro 12, I-56127 Pisa, Italy

Giorgio Biasiol

Laboratorio TASC, CNR–IOM, Area Science Park, I-34149 Trieste, Italy

(Received 27 July 2012; published 28 November 2012)

We report on the transition from the strong to the weak light-matter coupling regime between an intersubband excitation and a photonic crystal resonance in a nanostructured semiconductor membrane. Such a transition is induced by varying the intensity of an ultrafast light pulse, which is employed for pumping and probing the system eigenmodes. The phenomenon is interpreted in terms of the saturation of the intersubband transition due to the large number of photoexcited electrons in the quantum well, as confirmed by a thorough analysis performed both in frequency and time domain.

DOI: [10.1103/PhysRevB.86.201302](https://doi.org/10.1103/PhysRevB.86.201302)

PACS number(s): 71.36.+c, 42.50.Ct, 78.47.J–, 78.67.De

It has been almost a decade since the strong coupling regime between an intersubband (ISB) excitation in a semiconductor quantum well (QW) and the photonic resonance of a monolithic cavity embedding the heterostructure was reported.¹ The theory of the emerging quasiparticles (*intersubband polaritons*) is well understood in terms of the nonperturbative Hamiltonian coupling between the midinfrared or terahertz confined radiation and the electronic polarization field.^{2,3} The coupling strength is the *vacuum Rabi frequency*, which corresponds to half the spacing between the polariton modes, and whose value is proportional to the square root of the difference of surface charge density between the electronic subbands involved in the transition:

$$\Omega_R \propto \sqrt{n^{(1)} - n^{(2)}}. \quad (1)$$

From an experimental point of view, intersubband polaritons have been mainly probed by continuous wave (CW) measurements. Time-domain studies are described in few papers, which report on the nonadiabatic *creation* of polariton states induced by a near-infrared pump.^{4,5} In the present Rapid Communication we show how to *destroy* the intersubband polaritons on an ultrashort time scale ($\simeq 100$ fs) by means of a midinfrared light pulse whose spectrum covers both the upper and lower polaritonic branches at anticrossing. In synthesis, a certain number of polaritons are photoinjected, with the attendant creation of ISB excitations: Following Eq. (1), above a certain pulse intensity, the splitting is significantly decreased, and the concept of polaritons itself gets lost eventually. This phenomenon has been already observed in the exciton-polariton framework, where the terminology *polariton bleaching* was introduced.^{6,7} It should, however, be remarked that the saturation mechanisms are intrinsically different: While in the excitonic system it is the oscillator strength that is quenched by the electron-hole photoinduced plasma, in the intersubband case the leading effect is directly related to the saturation of a two-level system.^{8,9}

Interest in the intersubband polariton bleaching stems both from fundamental physics and from application perspectives. From the first point of view, the present work allows to determine the maximum resonant pumping rate above which polaritons start disappearing, which is important for deter-

mining the feasibility of excitation-induced phenomena such as the stimulated scattering between polariton states,¹⁰ and, at the same time, it permits to investigate the dynamics of light absorption and conversion into the quasiparticles. From the second, more application-oriented point of view, the analyzed samples exhibited the behavior of an ultrafast saturable absorber in the midinfrared spectral range, with an interesting potential for sensing and bistable devices.

The sample structure consists of a multiquantum well (MQW) GaAs/AlGaAs semiconductor heterostructure grown by molecular beam epitaxy on a [100] GaAs substrate, patterned with gold stripes and etched from the back side in order to obtain a free-standing membrane with a thickness of $2 \mu\text{m}$ and an area of $300 \times 300 \mu\text{m}^2$ [Fig. 1(a)]. The fabrication process is described elsewhere in more detail.¹¹ We realized two samples which differ by the doping in the quantum wells: One sample is undoped, while in the other silicon impurities in the wells provide a nominal electron density of $n_{\text{dop}} = 10^{12} \text{ cm}^{-2}$ in the first subband.

A preliminary sample characterization, consisting in the measurement of the dispersion of the bare photonic and polaritonic resonances, has been carried out on the undoped and the doped sample, respectively, as reported in Figs. 1(b) and 1(c). These maps were reconstructed from angle-resolved CW measurements performed with a Fourier-transform infrared spectrometer (FTIR) equipped with a glo-bar lamp and a HgCdTe (MCT) LN₂-cooled detector. The sample parameters (membrane thickness, gold stripe spacing, quantum well width) were designed in order to have the photonic resonance degenerate with the intersubband transition at an angle of 20° . Here and in the following it is assumed that the incident beam lies in a plane orthogonal to the metal stripes and that the light is *p*-polarized. The splitting of the single photonic branch in two polaritonic branches is a clear signature that in the doped sample the strong coupling regime is reached, with a Rabi energy of about 7 meV. Following Eq. (1), a difference in the surface charge density between the two subbands is responsible for such splitting. This has been quantified by fitting the experimental spectra with theoretical calculations obtained by the rigorous coupled-wave analysis (RCWA) method (scattering matrix method) detailed in Ref. 12. Here,

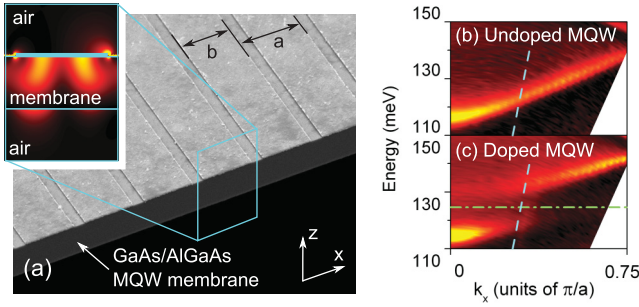


FIG. 1. (Color online) (a) Scanning electron micrograph of the sample, evidencing the semiconductor free-standing membrane patterned with gold stripes ($a = 4.3 \mu\text{m}$, $b = 0.8a$). The inset reports the resonant electric field intensity $|E_z|^2$ in the unit cell of the photonic crystal. (b) Photonic band structure measured by angle-resolved CW transmittance spectroscopy on a sample embedding undoped MQW. Angles up to 50° have been explored. (c) Same as (b), but from a doped sample. The dashed-dotted horizontal line highlights the intersubband transition energy, while the dashed lines indicate the free space light dispersion at the angle (20°) for which light and matter modes in the membrane become resonant.

the MQW is modeled as a dispersive uniaxial medium with

$$\varepsilon_x = \varepsilon_y = \varepsilon_{\parallel, \infty}, \quad (2)$$

$$\varepsilon_z^{-1} = \varepsilon_{z, \infty}^{-1} - \frac{1}{\varepsilon_W^2} \frac{4\pi e^2 (n^{(1)} - n^{(2)})}{m_0 (L_B + L_W)} \frac{1}{\tilde{\omega}_{12}^2 - \omega^2 - i\Gamma_{12}\omega}, \quad (3)$$

where $\varepsilon_{\parallel, \infty} = (L_B \varepsilon_B + L_W \varepsilon_W) / (L_B + L_W)$, $\varepsilon_{z, \infty}^{-1} = (L_B / \varepsilon_B + L_W / \varepsilon_W) / (L_B + L_W)$.¹³ The quantities $\varepsilon_B, \varepsilon_W$ (L_B, L_W) are the nominal barrier and well permittivities (thicknesses); the surface charge difference $n^{(1)} - n^{(2)}$, the depolarization-shifted intersubband transition energy $\hbar\tilde{\omega}_{12}$, and its half linewidth $\hbar\Gamma_{12}$ were regarded as fitting parameters. In these measurements we assumed $n^{(2)} = 0$, as the excitation density provided by the infrared lamp is small compared to the value of n_{dop} and since thermal excitation is negligible even under room temperature operation. From the fitting procedure, we thus found $n^{(1)} = 6.37 \times 10^{11} \text{ cm}^{-2}$, $\hbar\tilde{\omega}_{12} = 124.6 \text{ meV}$, and $\hbar\Gamma_{12} = 5.36 \text{ meV}$.

Bleaching of the polaritons in the doped sample was observed by illuminating the sample with $\approx 100 \text{ fs}$ pulsed light. We employed a system consisting of (i) a Ti:sapphire amplified laser (Coherent LIBRA) operated at a 5 kHz repetition rate with an average beam power of 1.5 W, (ii) an optical parametric amplifier (TOPAS) generating two near-infrared beams at wavelengths of about 1.5 and 1.7 μm , and (iii) a difference frequency generator (NDFG) which outputs a tunable pulse in the 10 μm wavelength range. For the present experiment the pulse spectrum was tuned so as to cover both polaritonic branches at anticrossing. The light beam, focused and collected with parabolic mirrors, was attenuated on a coarse intensity scale by using a set of neutral density filters; a fine tuning of the intensity on the sample was achieved by varying the distance between the sample and beam waist. By keeping the spot size always larger than the sample, we ensured a uniform intensity over the whole area of interest. Detection was provided by a FTIR, operated with a MCT detector and a lock-in amplifier. In Fig. 2(a) we report as dotted traces

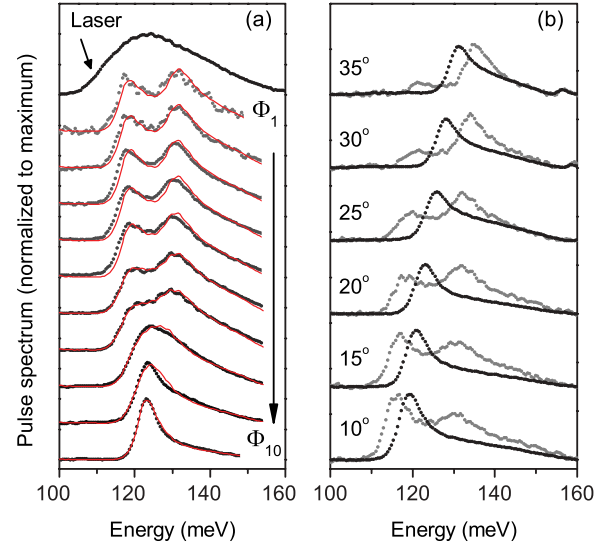


FIG. 2. (Color online) (a) Measured (dots) and fitting (lines) spectra of the ultrafast pulse for different incident photon fluxes and for a fixed incidence angle of 20° . At small flux the double peak is clear evidence of intersubband polaritons, while in the opposite case the single peak reveals the bare photonic nature of the excitation. The incident pulse spectrum is also reported for completeness. (b) Photonic vs polaritonic dispersion measured from ultrafast spectroscopy: The gray dotted lines represent the unbleached case (small flux), while the black dotted ones refer to the bleached case (high flux).

the spectra (namely, the Fourier transform of the autocorrelation) of the pulse after crossing the sample at different incident intensities. The upper trace corresponds to a photon flux $\Phi_1 = 10^{11} \text{ photons}/(\text{pulse cm}^2)$ (lowest intensity), while the lower trace to $\Phi_{10} = 1750 \times 10^{11} \text{ photons}/(\text{pulse cm}^2)$ (highest intensity); the pulse spectrum without the sample is also reported for completeness. Under the low intensity condition, the two-peaked polariton spectra already recorded in CW are observed; when the intensity is increased, the polariton bleaching clearly gives rise to a reduction in the splitting between the two peaks, which eventually merge into a single one. Further confirmation of the switching between strong and weak coupling regimes is gained by analyzing the angularly resolved spectra reported in Fig. 2(b), where gray traces are recorded under the lowest excitation intensity while black traces under the highest: Experimental evidence is that the polaritonic anticrossing doublet collapses in the single photonic resonance upon an intensity increase. A final remark regards the absolute intensities of the transmitted pulses: When the sample is bleached its absolute transmittance is about ten times larger than in the other case, making this system a good candidate for an application in saturable absorbers.

A quantitative analysis is performed by fitting the measured spectra with the RCWA method described above, assuming for $\hbar\tilde{\omega}_{12}$ the CW-measured value and leaving $(n^{(1)} - n^{(2)})$ and $\hbar\Gamma_{12}$ as fitting parameters. The nonradiative scattering rate is expected to be different from the CW-measured value since it is an excitation-dependent quantity, because of the Coulomb electron-electron interaction.¹⁴ A good agreement is obtained, as it can be observed in Fig. 2(a), although the theoretical

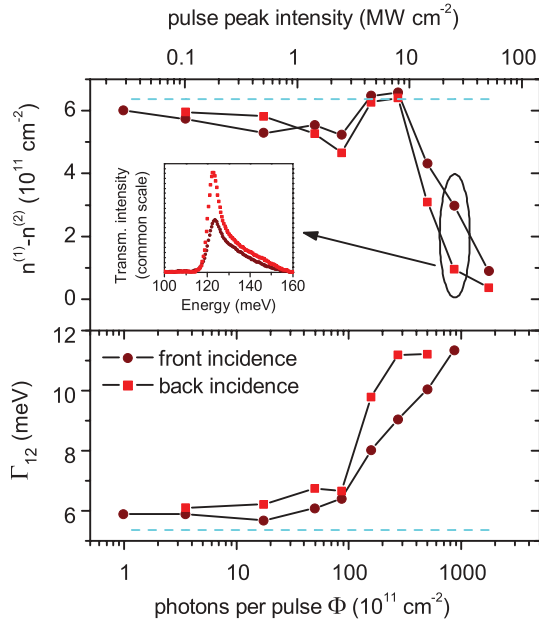


FIG. 3. (Color online) Saturation of the intersubband transition upon excitation intensity increase. The reduction of the surface charge density difference $n^{(1)} - n^{(2)}$ is the cause of polariton bleaching, and is accompanied by an increase in the nonradiative decay rate of the intersubband transition Γ_{12} . Dashed lines show for comparison the values found in CW low-intensity spectroscopy. *Front incidence* refers to light incoming from the gold stripe side of the membrane [see Fig. 1(a)]. The inset shows the transmitted pulse spectra where the front/back asymmetry is larger.

model treats the electromagnetic incident radiation as a plane wave—an assumption that is a relatively strong approximation of the experimental conditions of a few-cycle light pulse. As expected, the polariton bleaching corresponds to a reduction of the surface charge difference: The trend is reported in the upper panel of Fig. 3. Correspondingly, an increase in the scattering rate is observed (Fig. 3, lower panel). In those graphs, three regions can be identified. When $\Phi < 100 \times 10^{11} \text{ cm}^{-2}$, both $(n^{(1)} - n^{(2)})$ and $\hbar\Gamma_{12}$ are close to the CW values: The sample is far from the bleaching condition. As Φ is increased up to $500 \times 10^{11} \text{ cm}^{-2}$, a rapid growth in the scattering rate is observed, as expected.¹⁴ Meanwhile, the deviation from the decreasing trend in $(n^{(1)} - n^{(2)})$ may be partly considered an artifact stemming from the incomplete description of a transient phenomenon within a stationary plane-wave framework. A more accurate analysis of the experimental data, proposed in the following, will clarify the bleaching dynamics and justify the above reported behavior. Finally, the proper bleaching occurs in the range $\Phi = 500\text{--}1750 \times 10^{11} \text{ cm}^{-2}$, where $(n^{(1)} - n^{(2)})$ becomes close to zero. In this range the influence of Γ_{12} on the shape of the fitting spectra is negligible, hence no data points are reported in the lower panel of Fig. 3.

Although the global trend is the same for both front and back incidence (light incoming from the gold stripe side of the sample, or vice versa), an interesting asymmetry can be noticed. While linear optics would have given the same transmittance curves for both sides, due to the reciprocity theorem,¹⁵ a difference is reported here (see the inset of Fig. 3).

Indeed, it can be shown by RCWA calculation that—upon excitation with an incident field of given amplitude—the resonant electric field inside the photonic crystal has an intensity which is double when the sample is illuminated from the back side. As the surface charge difference depends on such an internal field intensity, bleaching would occur easier upon back illumination. We attribute to this asymmetry the differences observed in the range $\Phi = 500\text{--}1000 \times 10^{11} \text{ cm}^{-2}$.

In order to gain further insight into the bleaching process and to take full advantage of the data collected with an ultrafast source, we refined our picture by performing a short-time Fourier transform on the interferograms acquired with the FTIR for the case of front incidence. Our aim was to move beyond a simple frequency analysis and to gather informations also on the time-domain scale, thus observing the evolution of the bleaching process. The interferogram $I(\delta)$, where δ is the optical path difference between the interferometer arms, is convolved with the Gaussian (Gabor) wavelet $\exp(2\pi i\delta/\lambda) \exp[-(\delta - \delta_0 - ct)^2/2\Delta^2]$. As the wavelength λ and the time delay t are swept (δ_0 denotes the zero path difference), the full time-wavelength information contained in the signal are extracted.¹⁶ The wavelet full width at half maximum (FWHM) $\simeq 2\Delta$ has been set to 15 wavelengths at a central energy of 125 meV; this value corresponds to a temporal span of about 500 fs. A selection of short-time Fourier transforms is presented in Fig. 4 as contour plots, where wavelengths are converted to photon energies. Under the conditions of smallest or largest flux, Φ_1 and Φ_{10} , respectively, the sample is either fully unbleached or fully bleached, and no significant temporal evolution in the spectra is noticed (apart from the third peak appearing at 140 meV for Φ_1 , which may originate from measurement noise). On the contrary, when the photon flux lies in the transition region (Φ_7 and Φ_8), a

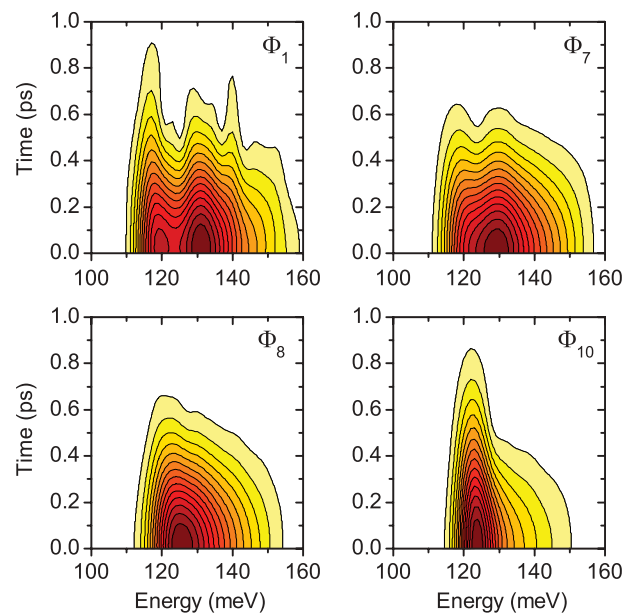


FIG. 4. (Color online) Short-time Fourier transforms of the interferograms at selected photon fluxes (see also Fig. 2). In the transition region, especially at Φ_7 , the sample exhibits a transition between the bleached and the unbleached states in the temporal domain.

temporal evolution of the spectral features is observed. The most relevant effect is found for Φ_7 , where a bifurcation is observed. We interpret this behavior as follows: The overall intensity of the incoming pulse is responsible for a partial bleaching, which is revealed by the single, broad peak of the spectrum observed for a zero time delay (corresponding to the interferogram centerburst, i.e., to the overlap of the most intense sections of the outgoing pulse). Meanwhile, the double-peaked spectra observed at time delays greater than a few hundred femtoseconds clearly indicate that the interferogram tail is characteristic of the unbleached state. As the interferogram tail derives from the overlap of the leading and the trailing part of the outgoing pulse, it can be inferred that at least in one of those time spans the sample is unbleached. In summary, when the incident pulse flux is in the transition region ($\Phi \simeq 500 \times 10^{11} \text{ cm}^{-2}$), the sample does not experience a steady bleached or unbleached state, while

it passes through intermediate, nonstationary states. This may be the reason for the nonsmooth trend reported in the upper panel of Fig. 3, which was obtained under the steady-state hypothesis.

In conclusion, we experimentally demonstrated that intersubband polaritons can be dynamically quenched on an ultrafast time scale, quantified in a few hundred femtoseconds. In addition, these results set an upper limit to the pump intensity that can be employed in optically pumped intersubband polariton experiments: For the present geometry, the limit is about 10^{13} photons/(pulse cm^2). Furthermore, a design for saturable absorbers in the midinfrared spectral range can be developed in these systems through an engineering of the device structure.

We gratefully acknowledge Simone De Liberato and Cristiano Ciuti for useful discussions.

*simone.zanotto@sns.it

¹D. Dini, R. Köhler, A. Tredicucci, G. Biasiol, and L. Sorba, *Phys. Rev. Lett.* **90**, 116401 (2003).

²C. Ciuti, G. Bastard, and I. Carusotto, *Phys. Rev. B* **72**, 115303 (2005).

³Y. Todorov, A. M. Andrews, R. Colombelli, S. De Liberato, C. Ciuti, P. Klang, G. Strasser, and C. Sirtori, *Phys. Rev. Lett.* **105**, 196402 (2010).

⁴G. Günter, A. A. Anappara, J. Hees, A. Sell, G. Biasiol, L. Sorba, S. De Liberato, C. Ciuti, A. Tredicucci, A. Leitenstorfer, and R. Huber, *Nature (London)* **458**, 178 (2009).

⁵M. Porer, J.-M. Ménard, A. Leitenstorfer, R. Huber, R. Degl'Innocenti, S. Zanotto, G. Biasiol, L. Sorba, and A. Tredicucci, *Phys. Rev. B* **85**, 081302 (2012).

⁶R. Houdré, J. L. Gibernon, P. Pellandini, R. P. Stanley, U. Oesterle, C. Weisbuch, J. O'Gorman, B. Roycroft, and M. Ilegems, *Phys. Rev. B* **52**, 7810 (1995).

⁷T. B. Norris, J. K. Rhee, D. S. Citrin, M. Nishioka, and Y. Arakawa, *Il Nuovo Cimento* **17**, 1295 (1995).

⁸F. H. Julien, J.-M. Lourtioz, N. Herschkorn, D. Delacourt, J. P. Pocholle, M. Papuchon, R. Planel, and G. L. Roux, *Appl. Phys. Lett.* **53**, 116 (1988).

⁹J. Y. Duboz, E. Costard, E. Rosencher, P. Bois, J. Nagle, J. M. Berset, D. Jaroszynski, and J. M. Ortega, *J. Appl. Phys.* **77**, 6492 (1995).

¹⁰S. De Liberato and C. Ciuti, *Phys. Rev. Lett.* **102**, 136403 (2009).

¹¹R. Degl'Innocenti, S. Zanotto, A. Tredicucci, G. Biasiol, and L. Sorba, *Solid State Commun.* **151**, 1725 (2011).

¹²S. Zanotto, G. Biasiol, R. Degl'Innocenti, L. Sorba, and A. Tredicucci, *Appl. Phys. Lett.* **97**, 231123 (2010).

¹³M. Załuźny and C. Nalewajko, *Phys. Rev. B* **59**, 13043 (1999).

¹⁴R. A. Kaindl, K. Reimann, M. Woerner, T. Elsaesser, R. Hey, and K. H. Ploog, *Phys. Rev. B* **63**, 161308 (2001).

¹⁵The reciprocity theorem states that the transmitted amplitude remains unchanged if the source and detector are exchanged, provided that the scatterer is constituted by linear media with symmetric permeability and permittivity tensors [see, e.g., R. Potton, *Rep. Progr. Phys.* **67**, 717 (2004)].

¹⁶E. Stade, *Fourier Analysis* (Wiley-Interscience, New York, 2005).